Supporting Information:

"Living" Luminogens: Light Driven ACQ-to-AIE Transformation Accompanied with Solid-State Actuation

Haoran Wang, ‡[ab] Hao Xing, ‡[a] Junyi Gong,[a] Haoke Zhang,[a] Jun Zhang,[a] Peifa Wei,[a] Guojian Yang,[b] Jacky W. Y. Lam,[a] Ran Lu,*[,b] and Ben Zhong Tang* [acd]

[a] Department of Chemistry, Hong Kong Branch of Chinese National Engineering Research Center for Tissue Restoration and Reconstruction and Institute for Advanced Study, and Institute for Advanced Study, The Hong Kong University of Science and Technology, Clear Water Bay, Kowloon, Hong Kong, China. E-mail: tangbenz@ust.hk

[b] State Key Laboratory of Supramolecular Structure and Materials, College of Chemistry, Jilin University, Changchun 130012, P. R. China. E-mail: luran@jlu.edu.cn

[c] HKUST-Shenzhen Research Institute, No.9 Yuexing first RD, South Area, Hi-tech Park, Nanshan, Shenzhen 518057, China.

[d] Center for Aggreagtion-Induced Emission, SCUT-HKUST Joint Research Institute, State Key Laboratory of Luminescent Materials and Devices, South China University of Technology, Guangzhou 510640, China.

Table of Content

Experimental Section

Materials

All the chemicals and spectroscopic grade solvents such as dichloromethane (DCM), hexane, dimethyl sulfoxide (DMSO) were procured from Merck Company and used without further purification. *trans*-2-(4-Fluorostyryl)benzo[*d*]oxazole (*t*-FSBO) and *trans*-2-(2,4-difluorostyryl)benzo[*d*]oxazole (*t*-2FSBO) were synthesized according to a previous report.[1]

Characterization

^{1}H and ^{13}C NMR spectra were recorded on a Bruker ARX 400 NMR spectrometer using deuterated DMSO and tetramethyl silane (TMS; δ = 0 ppm) as internal reference. UV/vis absorption spectra were recorded on Shimadzu 2550 UV/vis spectrophotometer. The photoluminescence (PL) spectra were recorded on a Horiba Fluorolog-3 spectrofluorometer. The absolute fluorescence quantum yield was measured by a calibrated integrating sphere (Labsphere). High-resolution mass spectroscopy (HRMS) was carried out on a GCT premier CAB048 mass spectrophotometer operating in MALDI-TOF mode. Gel filtration chromatography was performed using an Agilent 5 Prep-C18 column conjugated to an Agilent 1260 Infinite HPLC system. Before running, each sample was purified *via* 0.22 μm filter to remove any aggregates. The flow rate was fixed at 40 mL/min, the injection volume was 250 μL and each sample was run for 6 min. The absorption wavelength used was set at 250 nm. Acetonitrile/water (85/15, *v*/*v*) cosolvent was used as the running buffer. Single-crystal data was collected on a Bruker Smart APEXII charge-coupled device (CCD) diffractometer using graphite

monochromated Cu Kα radiation (λ = 1.54178 Å). The structures were solved by the direct methods and refined on F2 by full-matrix least-square using the SHELXTL-97 program.[2] X-ray diffraction (XRD) pattern was collected on an X'per Pro (PANalytical) instrument with Cu Kα radiation (λ = 1.5418 Å) at 25 °C (scan range: 5–30°). The samples for XRD measurements were prepared by casting the solution on silica wafer and freeze-dried. The flashlight (365 nm, 3 W) was used as UV light source in photo-cycloaddition studies and the irradiation intensity is about 35 mW/cm^2.

Calculation

All quantum mechanism (QM) calculations were performed on ORCA 4.1 package. The equilibrium structures of all mentioned compounds in the ground state and the excited state were optimized under BLYP pure functional with def2-SVP basis set and RI-approximation. The vertical excitation energy of different geometries was obtained under PBE0 hybrid functional with def2-SVP basis set. The wavefunction analysis, including electron density difference, HOMO–LUMO distribution, and RDG analysis were calculated on multifunctional wavefunction software Multiwfn 3.6.[3,4]

Film Preparation

Film in Figure 5c, that is, the *t*-FSBO film on glove was prepared by the following procedures. *t*-FSBO solution in DCM (c = 0.01 mol/L) was initially prepared. The lab-used nitrile butadiene rubber glove was then cut into small thin pieces. After infiltrating the thin glove into the *t*-FSBO solution for few seconds, the *t*-FSBO film on glove was obtained and dried for use. Different kinds of substrates such as polymer (polydimethylsiloxane, PDMS), weighing paper, filter paper, and others are also tried to prepare t-FSBO films in order to show the macroscopic motion. Since the glove shows the highest contrast and best mobility, we chosen the t-FSBO film on glove for demonstration. This is due to the better alignment and packing of t-FSBO molecules on glove when compared with other substrates.

Characterization of *t*-FSBO

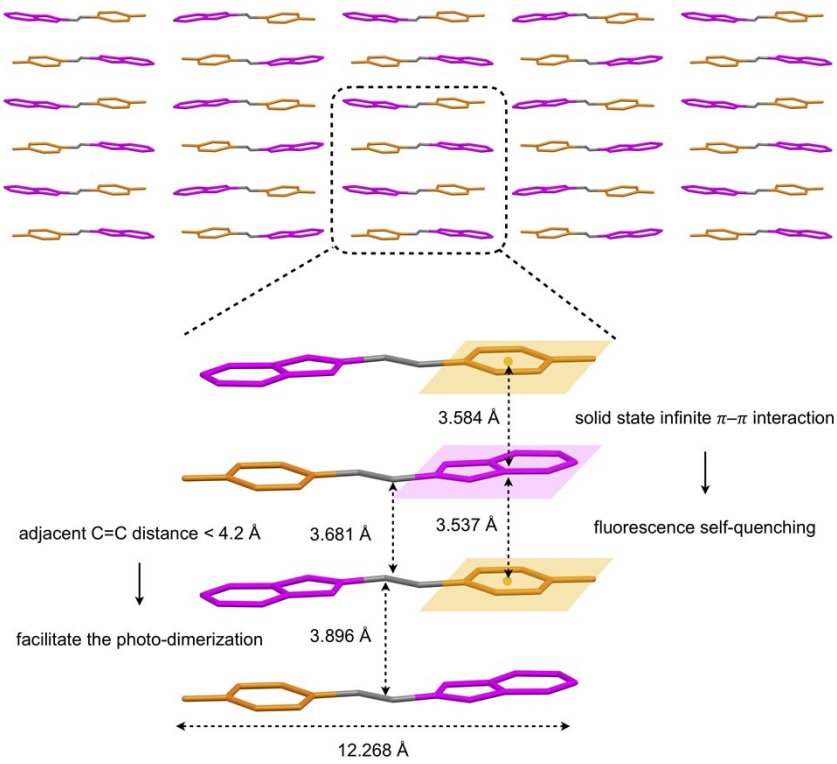

Figure S1. Single crystal structure of *t*-FSBO and the distance between two adjacent parallel molecules.

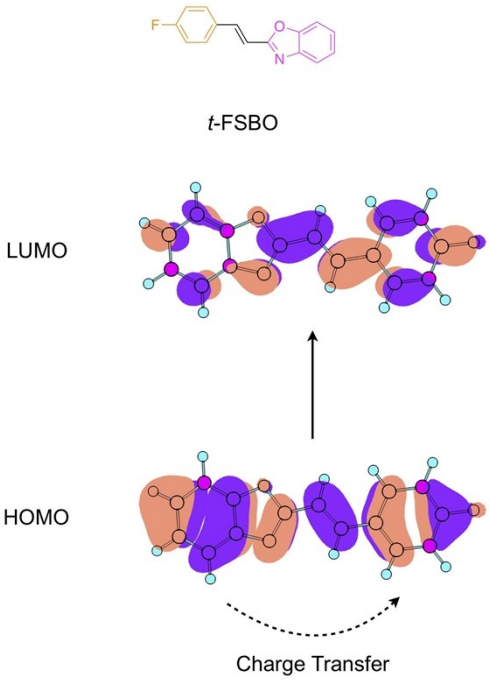

Figure S2. Electron cloud distribution and energy levels of *t*-FSBO in the ground state, ORCA 4.1 package.

Photo-cycloaddition Process of *t*-FSBO

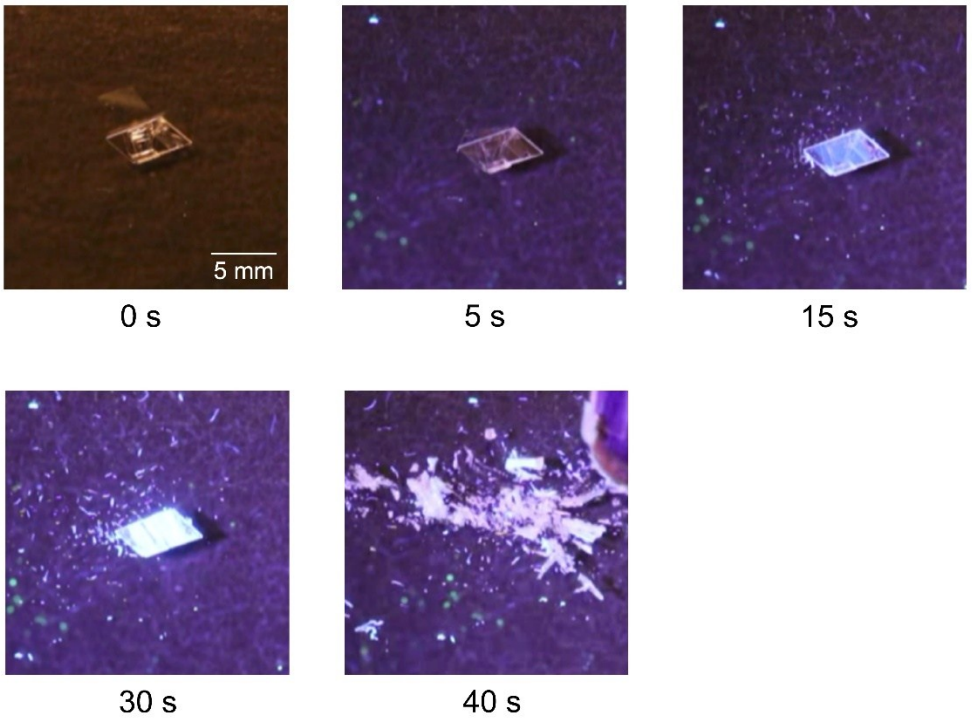

Figure S3. Photos of a *t*-FSBO bulk crystal before and after irradiated by 365 nm for different time.

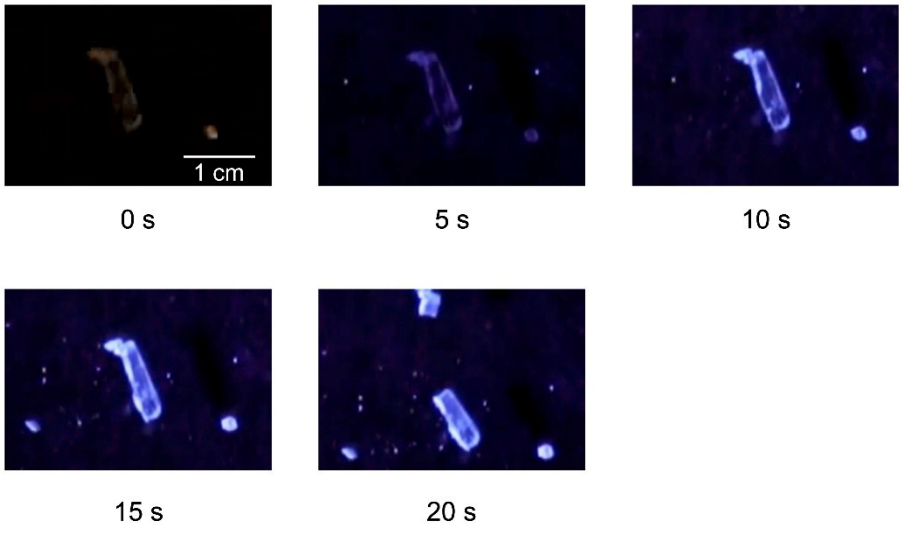

Figure S4. Photos of *t*-FSBO before and after irradiated by 365 nm for different time in vacuum and dry condition.

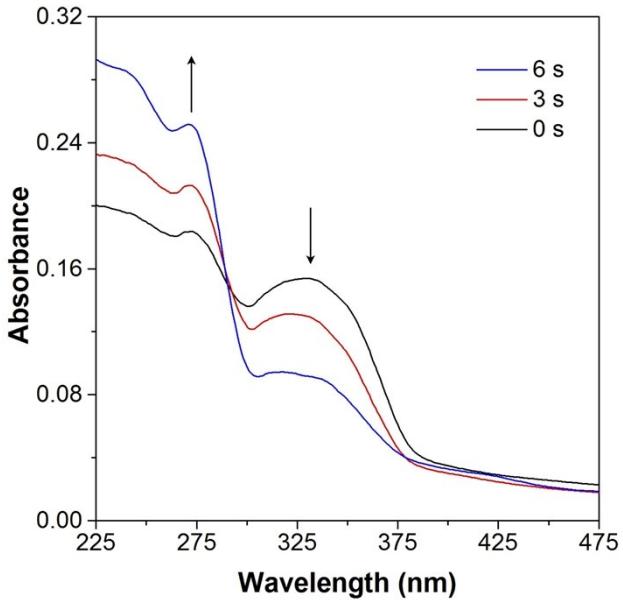

Figure S5. UV-vis absorption spectra of *t*-FSBO microcrystals before and after irradiated by 365 nm light for different time.

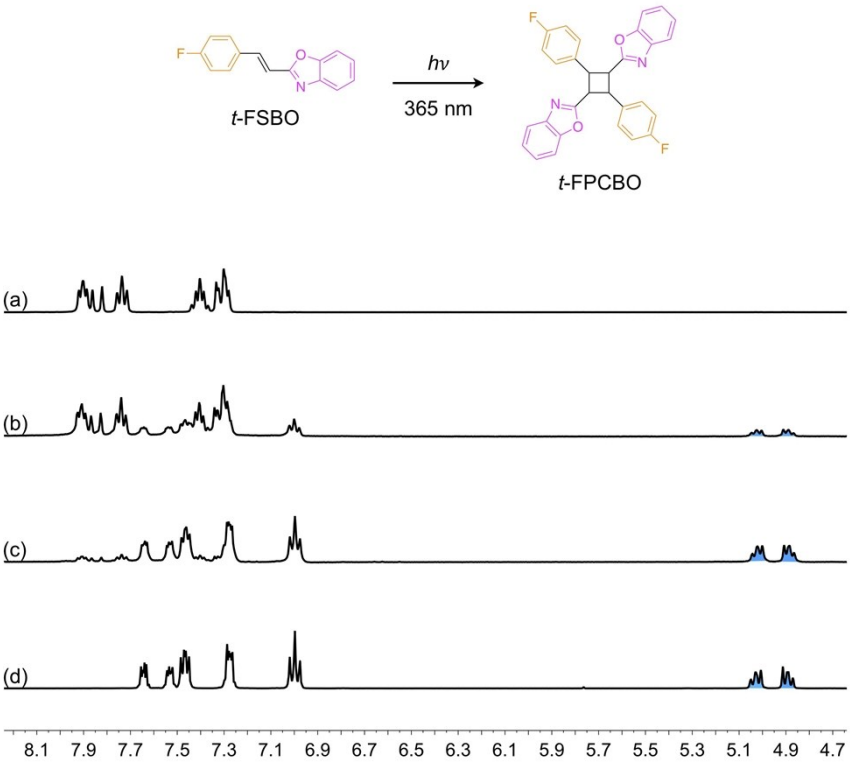

Figure S6. Partial ^{1}H NMR spectra (400 MHz, 298 K, DMSO-d_6) of *t*-FSBO microcrystals (a) directly dissolved in DMSO-d_6 and (b and c) dissolved in DMSO-d_6 after irradiated by 365 nm UV for (b) 2 min and (c) 4 min. (d) Partial ^{1}H NMR spectrum of recrystallized *t*-FSBO in DMSO-d_6 after irradiation by 365nm UV for 10 min.

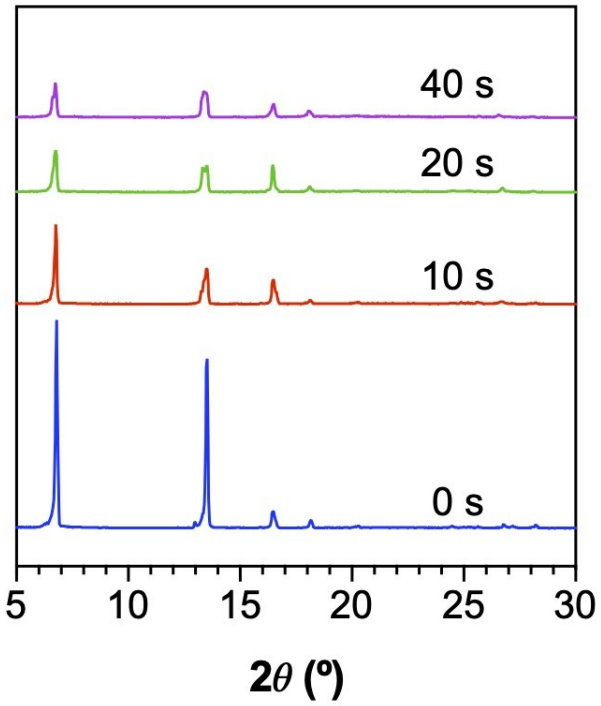

Figure S7. XRD patterns of *t*-FSBO microcrystals under 365 nm irradiation for different time.

Preparation and Characterizations of *t*-FPCBO

Scheme S1. Synthetic route to *t*-FPCBO.

transoid-2,2'-(2,4-bis(4-fluorophenyl)cyclobutene-1,3-diyl)bis(benzo[*d*]oxazole) (*t*-FPCBO)

t-FSBO powder (300 mg, 1.25 mmol) was added into grinding bowl and irradiated under the 365 nm UV light (20 mw/cm^3) with grinding and stirring for 20 min at room temperature until blue fluorescence was observed. The crude product was purified by column chromatography (silica gel) using ethyl acetate/hexane mixture (*v*/*v* = 1/10) as eluent. White solid of *t*-FPCBO (0.20 g, 67%) was obtained in a yield of 67%. M.P. 192.0–193.0 °C. ^{1}H NMR (400 MHz, DMSO-d_6, 298 K), δ (ppm): 7.68–7.61 (m, 2H), 7.57–7.50 (m, 2H), 7.47 (dd, J = 8.5, 5.5 Hz, 4H), 7.28 (dd, J = 5.9, 3.2 Hz, 4H), 7.00 (t, J = 8.8 Hz, 4H), 5.08–4.98 (m, 2H), 4.89 (dd, J = 9.9, 7.1 Hz, 2H). ^{13}C NMR (100 MHz, DMSO-d_6, 298 K), δ (ppm): 164.83 (s), 163.06 (s), 160.61 (s), 150.90 (s), 140.80 (s), 133.53 (d, J = 3.2 Hz), 128.89 (d, J = 8.1 Hz), 124.83 (s), 124.23 (s), 119.74 (s), 115.43 (s), 115.22 (s), 110.28 (s), 43.63 (s), 42.17 (s). HRMS (MALDI-TOF), *m*/*z*: [M + H] calcd for $C_{30}H_{21}F_2N_2O_2$, 479.1493, found 479.1543.

The single crystal structure of *t*-FPCBO was already shown in Figure 1e and the corresponding crystal data was shown in Table S1.

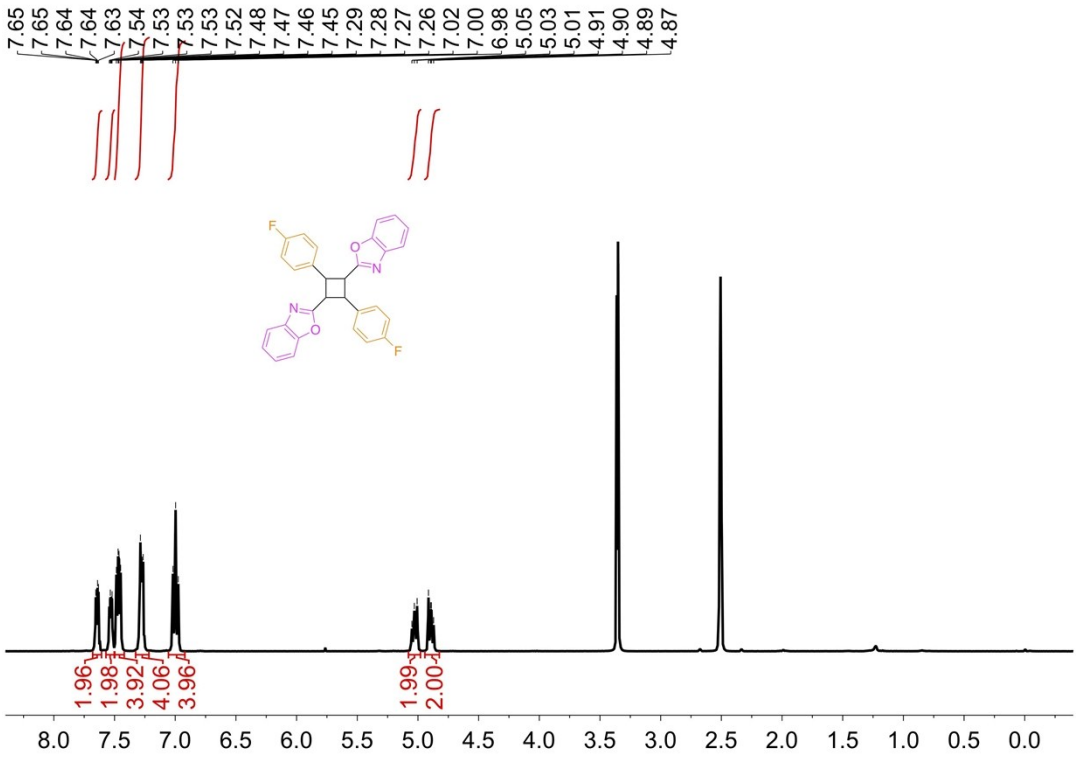

Figure S8. ^{1}H NMR (400 MHz, 298 K) spectrum of *t*-FPCBO in DMSO-d_6.

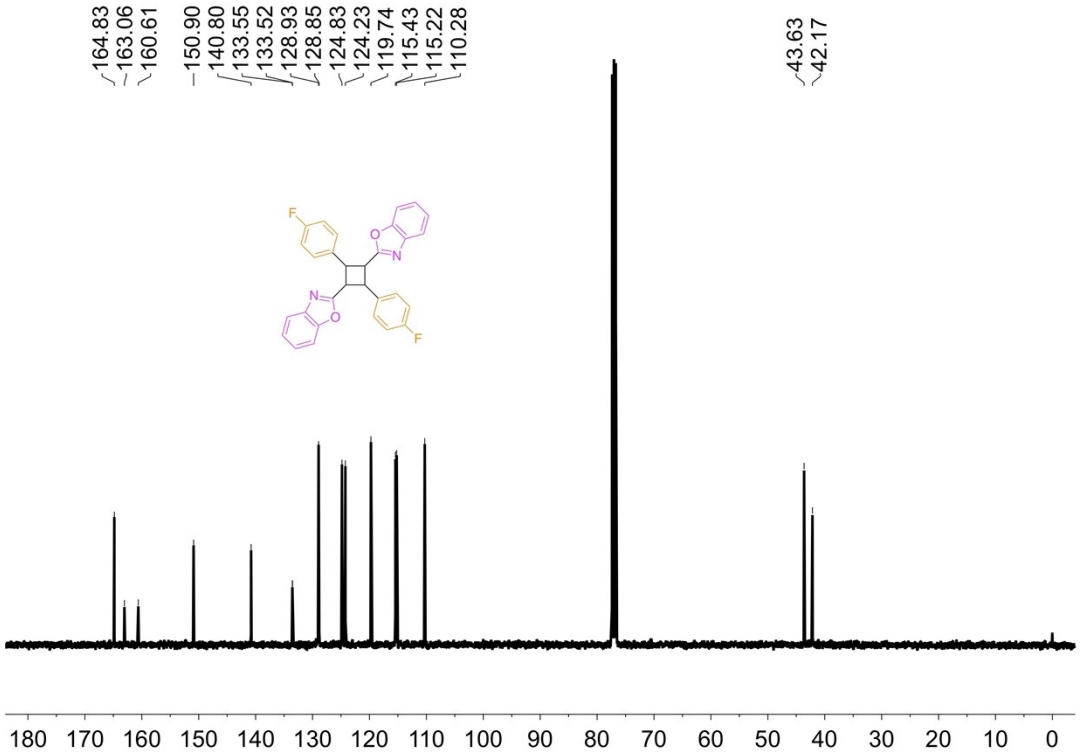

Figure S9. ^{13}C NMR (100 MHz, 298 K) spectrum of *t*-FPCBO in DMSO-d_6.

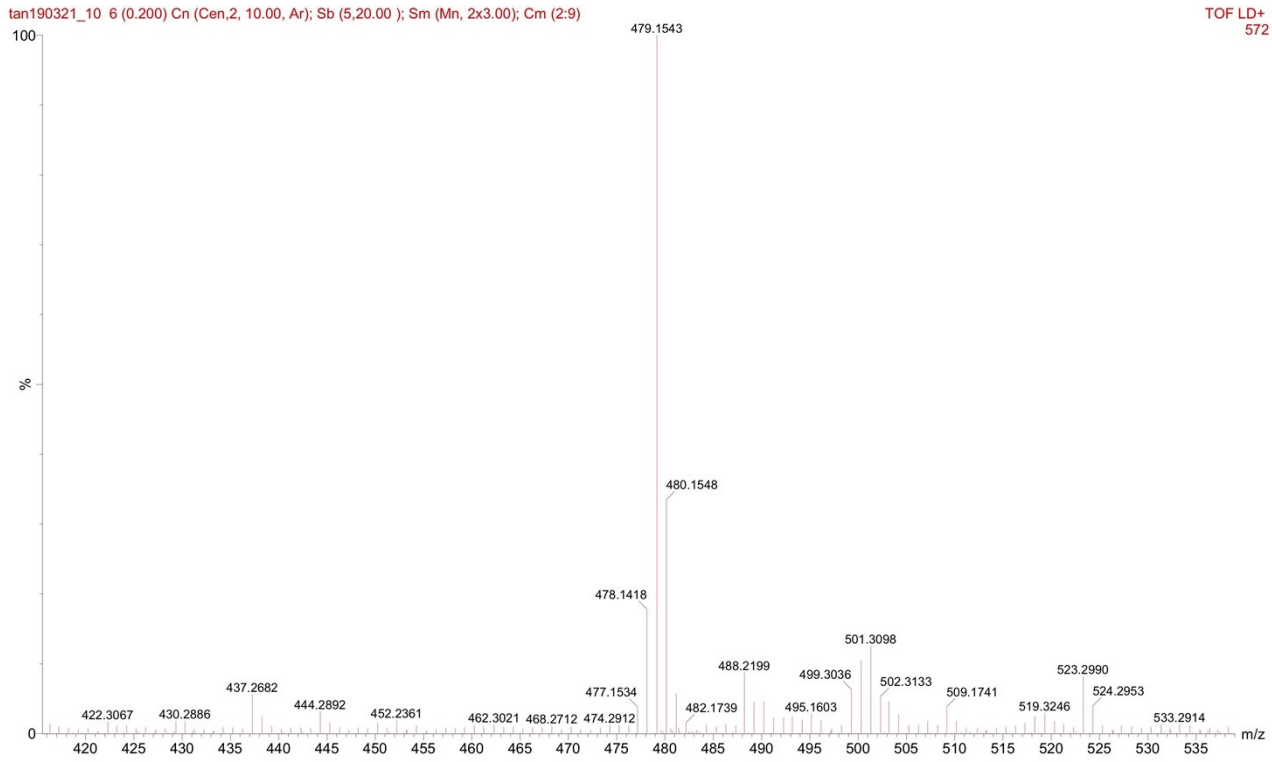

Figure S10. High-resolution mass spectrum of *t*-FPCBO.

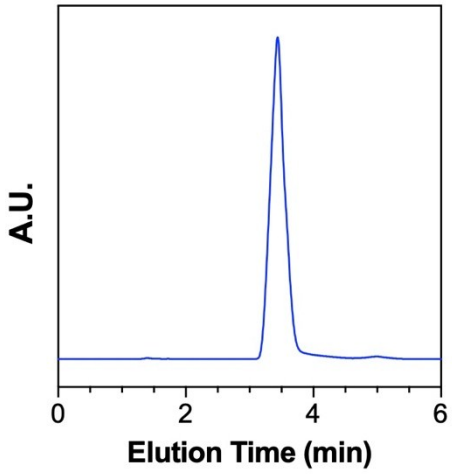

Figure S11. HPLC spectrum of *t*-FPCBO in acetonitrile solution.

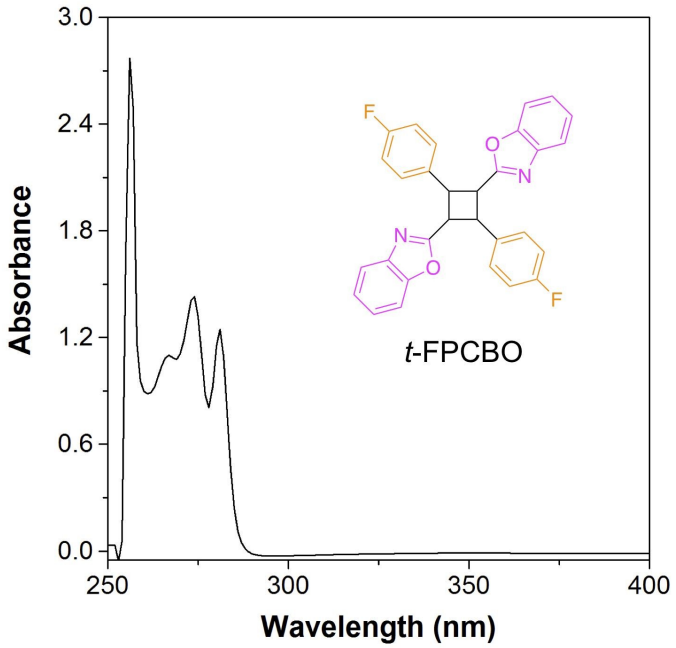

Figure S12. UV-vis absorption spectrum of *t*-FPCBO in CH_2Cl_2, $c = 1.0 \times 10^{-5}$ M.

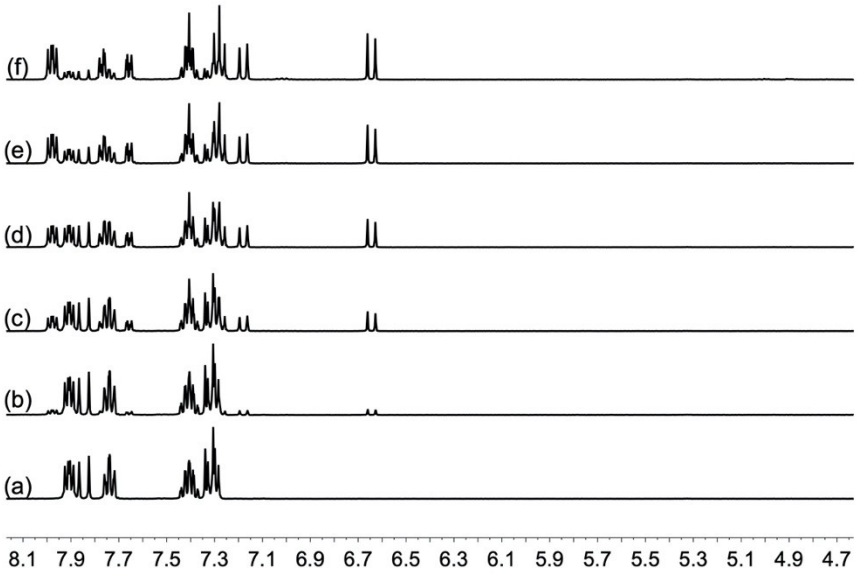

Figure S13. Partial ^{1}H NMR spectra (400 MHz, 298 K, DMSO-d_6) of *t*-FSBO in DMSO-d_6 solution after irradiated by 365 nm UV for (a) 0 s, (b) 10 s, (c) 20 s, (d) 60 s, (e) 120 s, and (f) 300 s.

Table S1. Crystal data and structure refinement for *t*-FPCBO.

	t-FPCBO
CDCC	1850301
Formula weight	478.48
Sp. Group	P21/C
Crystal system	monoclinic
a (Å)	21.7576(3)
b (Å)	9.38142(11)
c (Å)	22.7647(3)
α (deg)	90
β (deg)	99.6152(11)
γ (deg)	90
V (Å^3)	4581.40(9)
Z	8
Dcalc (g/cm^3)	1.387
μ (mm^{-1})	0.814
Final R indices [I > 2sigma(I)]	R1 = 0.0482, wR2 = 0.1112
R indices (all data)	R1 = 0.0447, wR2 =0.1139
GoF	1.027

Photophysical Properties and Characterizations of *t*-2FSBO

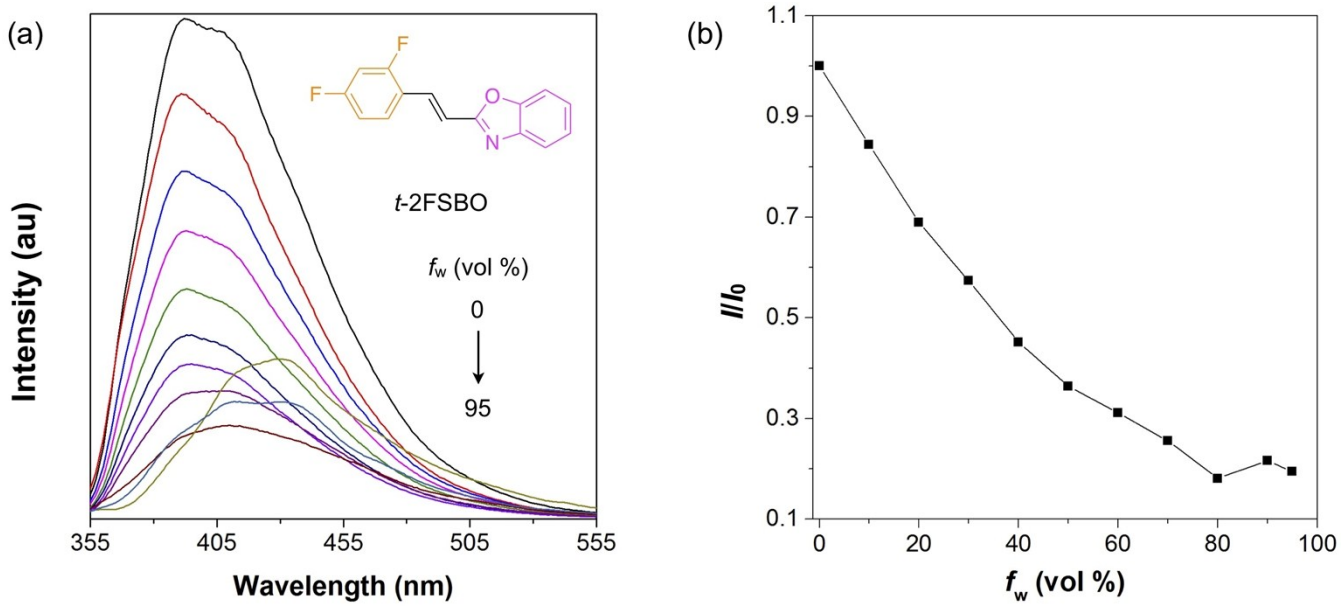

Figure S14. (a) PL spectra of *t*-2FSBO in DMSO/water mixtures with different water fractions (f_w). (b) Plots of relative PL intensity (I/I_0) at 394 nm *versus* f_w. $c = 1\times10^{-5}$ M, $\lambda_{ex} = 330$ nm.

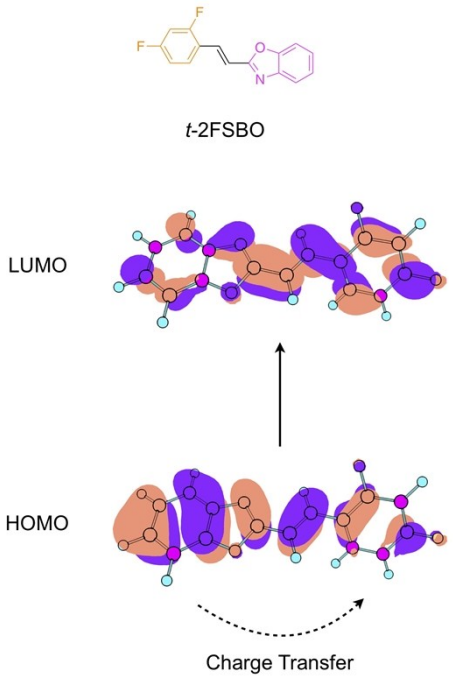

Figure S15. Electron cloud distribution and energy levels of *t*-2FSBO in the ground state, ORCA 4.1 package.

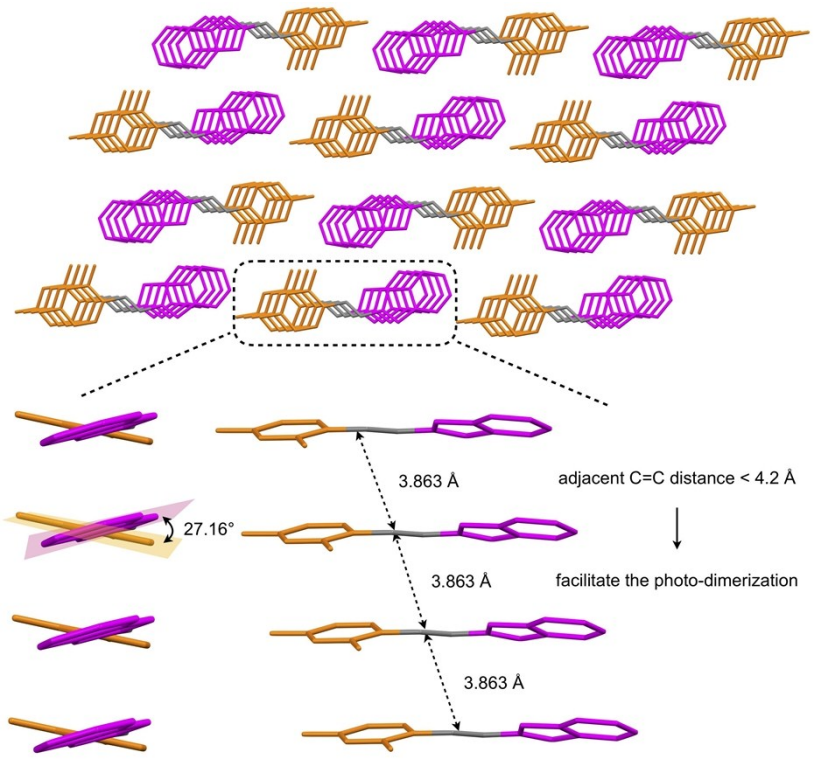

Figure S16. Single crystal structure of *t*-2FSBO and the distance between two adjacent parallel molecules.

Photo Cycloaddition Process of *t*-2FSBO

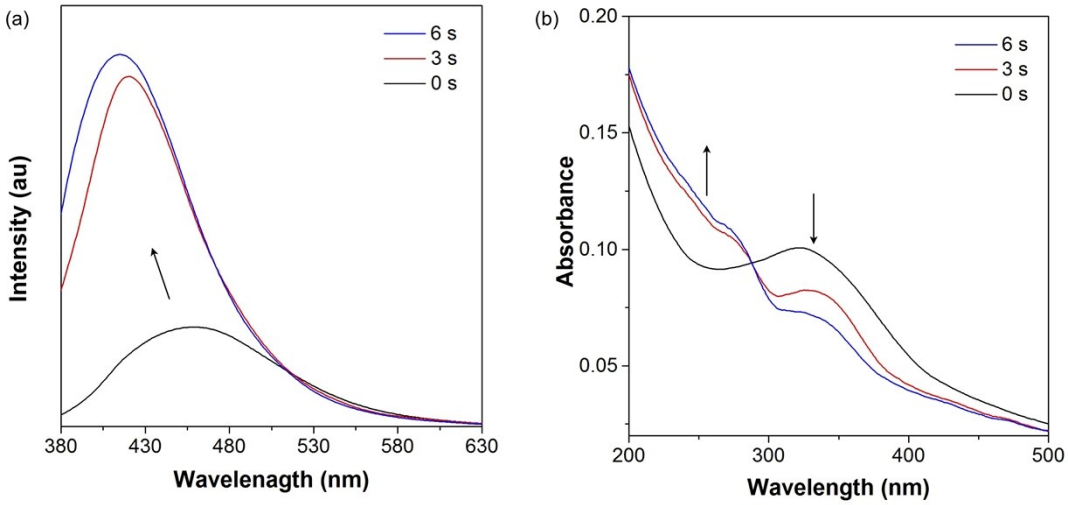

Figure S17. (a) Fluorescence and (b) UV-vis absorption spectra of *t*-2FSBO microcrystals before and after irradiated by 365 nm light for different time.

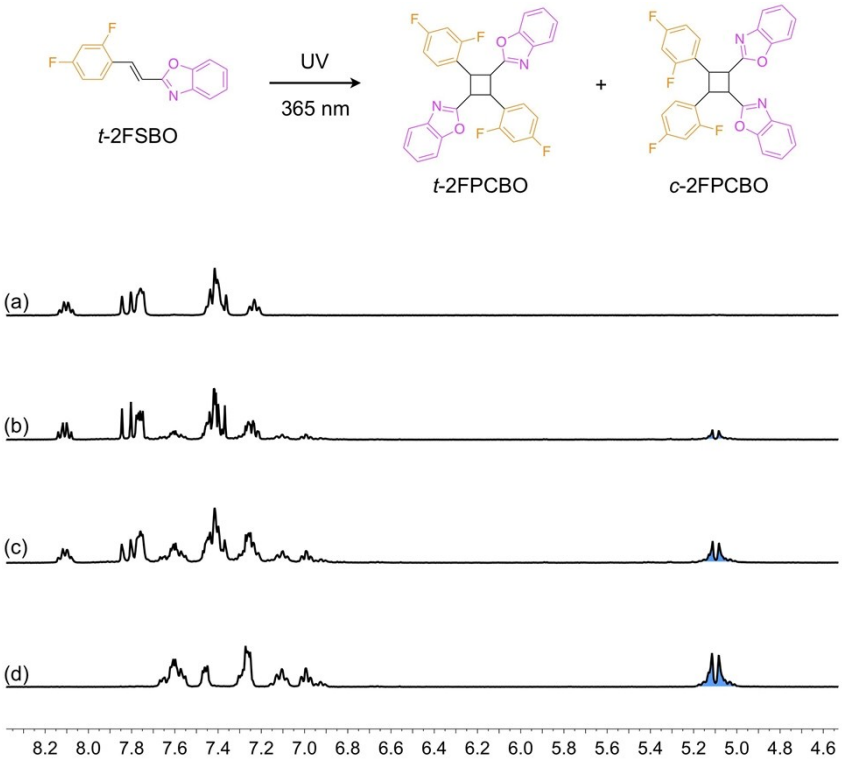

Figure S18. Partial ^{1}H NMR spectra (400 MHz, 298 K, DMSO-d_6) of *t*-2FSBO microcrystals (a) directly dissolved in DMSO-d_6 and (b and c) dissolved in DMSO-d_6 after irradiated by 365 nm UV light for (b) 2 min and (c) 4 min. (d) Partial ^{1}H NMR spectrum of recrystallized *t*-2FSBO dissolved in DMSO-d_6 after irradiated by 365nm UV light for 10 min.

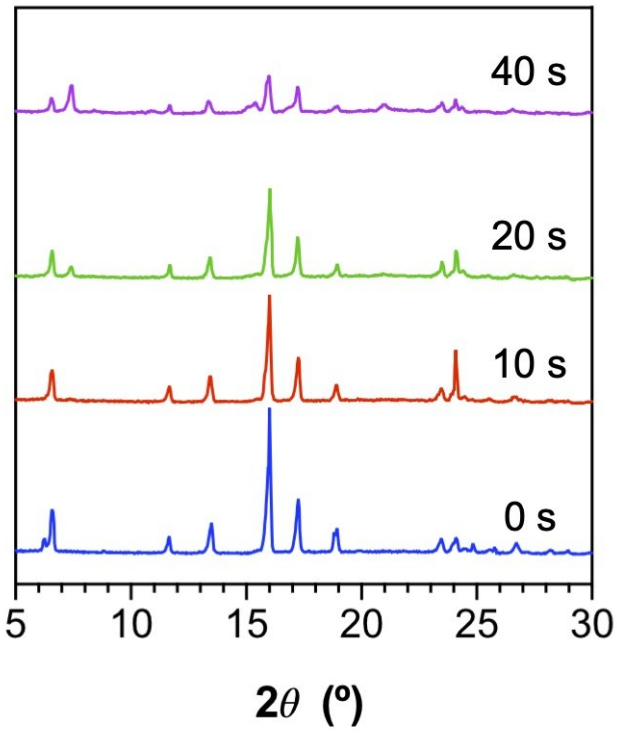

Figure S19. XRD patterns of *t*-2FSBO microcrystals under 365 nm irradiation for different time.

Preparation and Characterizations of *t*-2FPCBO and *c*-2FPCBO

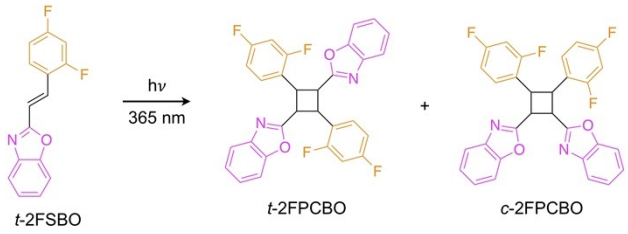

Scheme S2. Synthetic route to *t*-2FPCBO and *c*-2FPCBO.

transoid-2,2'-(2,4-bis(2,4-fluorophenyl)cyclobutene-1,3-diyl)bis(benzo[*d*]oxazole) (*t*-2FPCBO) and *cisoid*-2,2'-(3,4-bis(2,4-fluorophenyl)cyclobutene-1,2-diyl)bis(benzo[*d*]oxazole) (*c*-2FPCBO)

t-2FSBO powder (300 mg, 1.16 mmol) was added into grinding bowl and irradiated under 365 nm UV light (20 mw/cm^3) with grinding and stirring for 20 min at room temperature until blue fluorescence was observed. The crude product was purified by column chromatography (silica gel) using ethyl acetate/hexane mixture (*v*/*v* = 1/10) as eluent. White solid of *t*-2FPCBO (20 mg) and white solid of *c*-2FPCBO were obtained in a total yield of 73%.

t-2FPCBO: M.P. 202.0–203.0 °C. ^{1}H NMR (400 MHz, DMSO-d_6, 298 K), δ (ppm): 7.74–7.59 (m, 4H), 7.59–7.49 (m, 2H), 7.33–7.27 (m, 3H), 7.19–7.08 (m, 2H), 6.93 (t, J = 8.6 Hz, 2H), 5.20–5.10 (m, 2H), 5.07–4.98 (m, 2H). ^{13}C NMR (100 MHz, DMSO-d_6, 298 K), δ (ppm): 165.09 (d, J = 14.8 Hz), 150.88 (s), 140.80 (s), 125.61 (s), 124.87 (s), 121.58 (s), 120.02 (s), 118.32 (s), 110.84 (s), 39.06 (s), 38.11 (s). HRMS (MALDI-TOF), *m*/*z*: [M–F–H] calcd for $C_{30}H_{18}F_3N_2O_2$, 495.1399, found 495.1350.

c-2FPCBO: M.P. 206.0–207.0 °C. ^{1}H NMR (400 MHz, DMSO-d_6, 298 K), δ (ppm): 7.66–7.54 (m, 4H), 7.50–7.41 (m, 2H), 7.30–7.22 (m, 4H), 7.09 (dd, J = 13.6, 6.0 Hz, 2H), 6.99 (td, J = 8.5, 2.5 Hz, 2H), 5.10 (d, J = 10.6 Hz, 4H). ^{13}C NMR (100 MHz, DMSO-d_6, 298 K), δ (ppm): 165.59 (s), 150.87 (s), 140.83 (s), 134.78 (d, J = 2.9 Hz), 129.95 (d, J = 8.0 Hz), 125.35 (s), 124.73 (s), 119.87 (s), 115.44 (s), 115.23 (s), 110.89 (s), 43.26 (s), 41.66 (s). HRMS (MALDI-TOF), *m*/*z*: [M–F–H] calcd for $C_{30}H_{18}F_3N_2O_2$, 495.1399, found 495.1298.

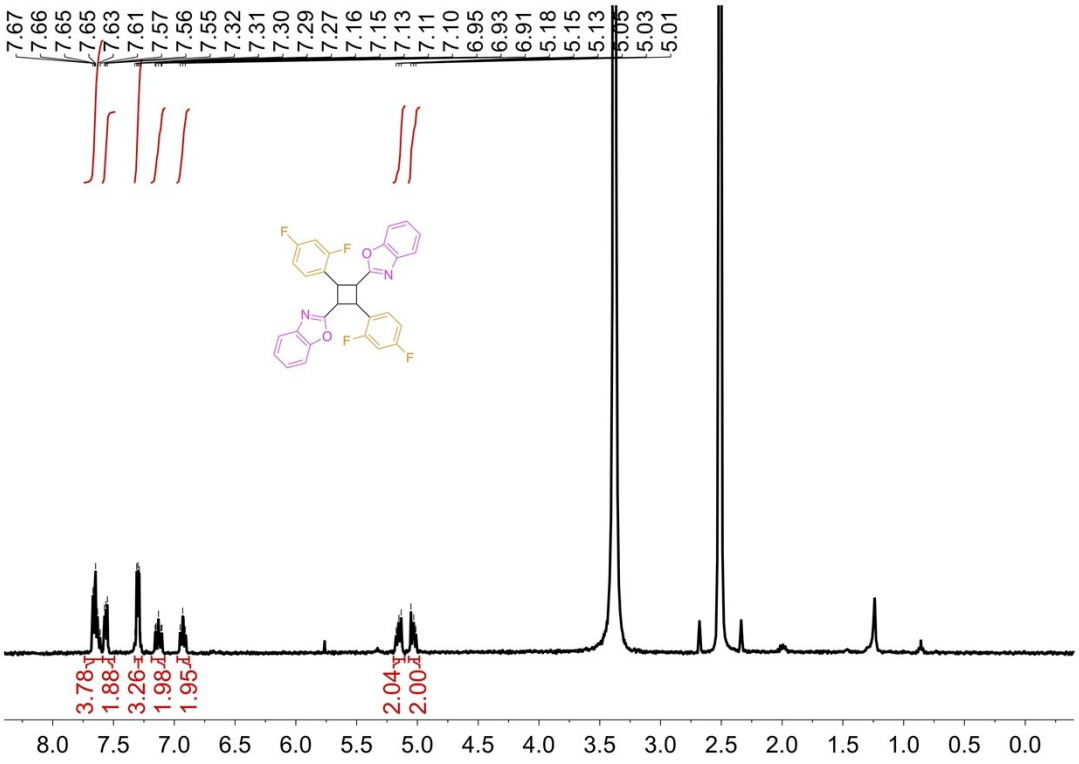

Figure S20. ^{1}H NMR (400 MHz, 298 K) spectrum of *t*-2FPCBO in DMSO-d_6.

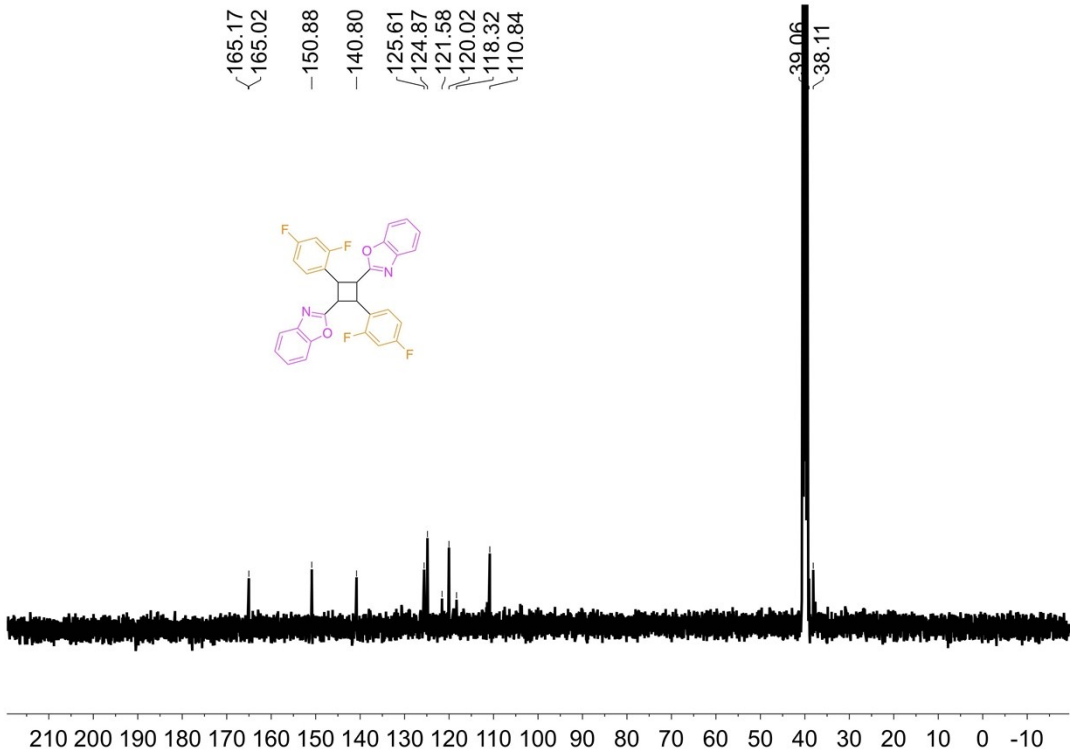

Figure S21. ^{13}C NMR (100 MHz, 298 K) spectrum of *t*-2FPCBO in DMSO-d_6.

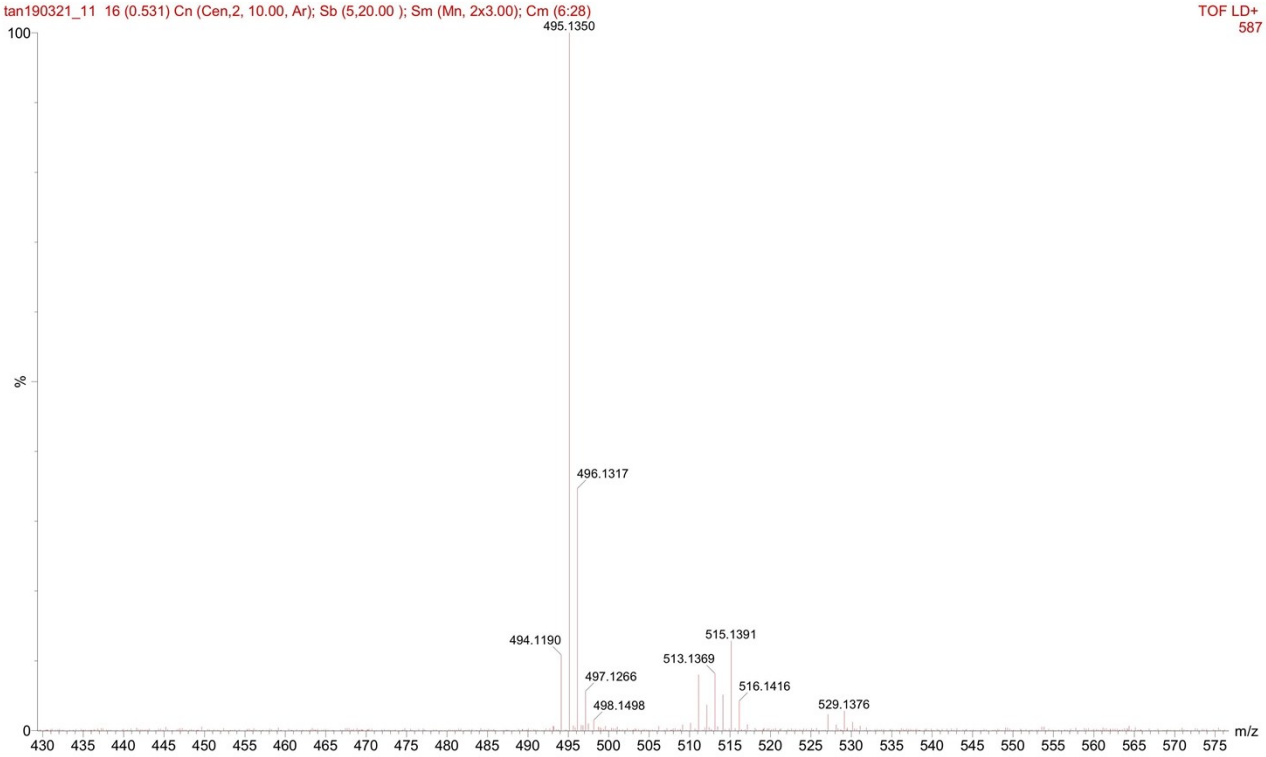

Figure S22. High-resolution mass spectrum of *t*-2FPCBO.

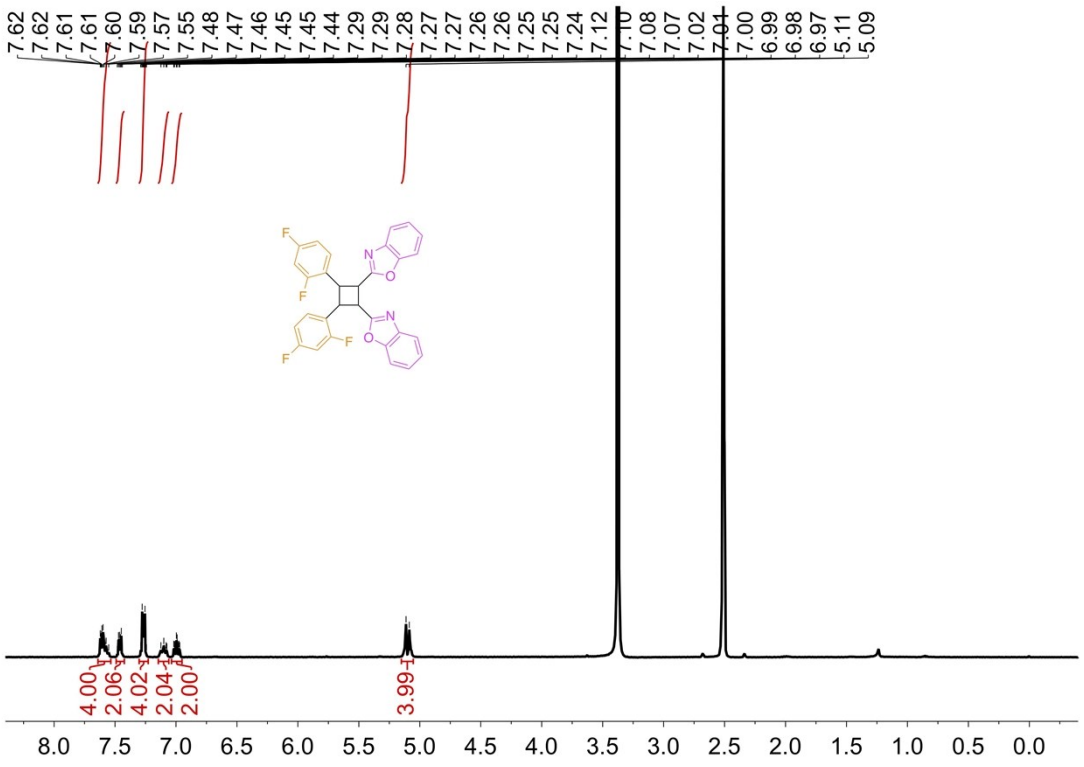

Figure S23. ^{1}H NMR (400 MHz, 298 K) spectrum of *c*-2FPCBO in DMSO-d_6.

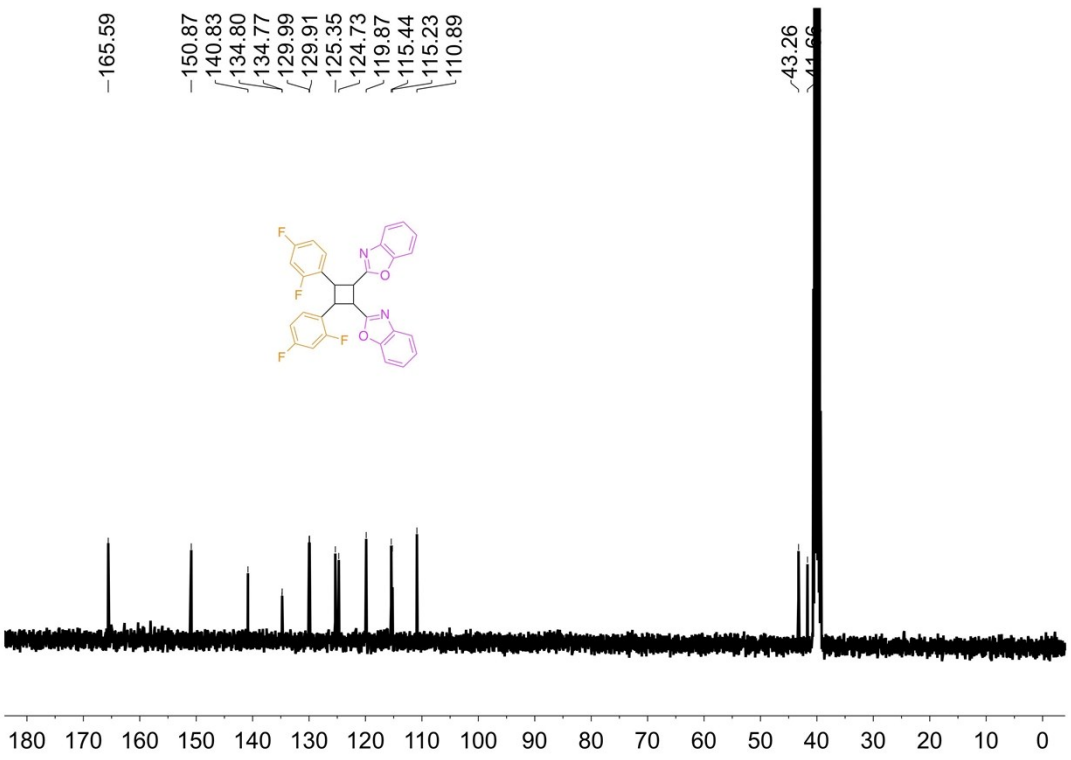

Figure S24. ^{13}C NMR (100 MHz, 298 K) spectrum of *c*-2FPCBO in DMSO-d_6.

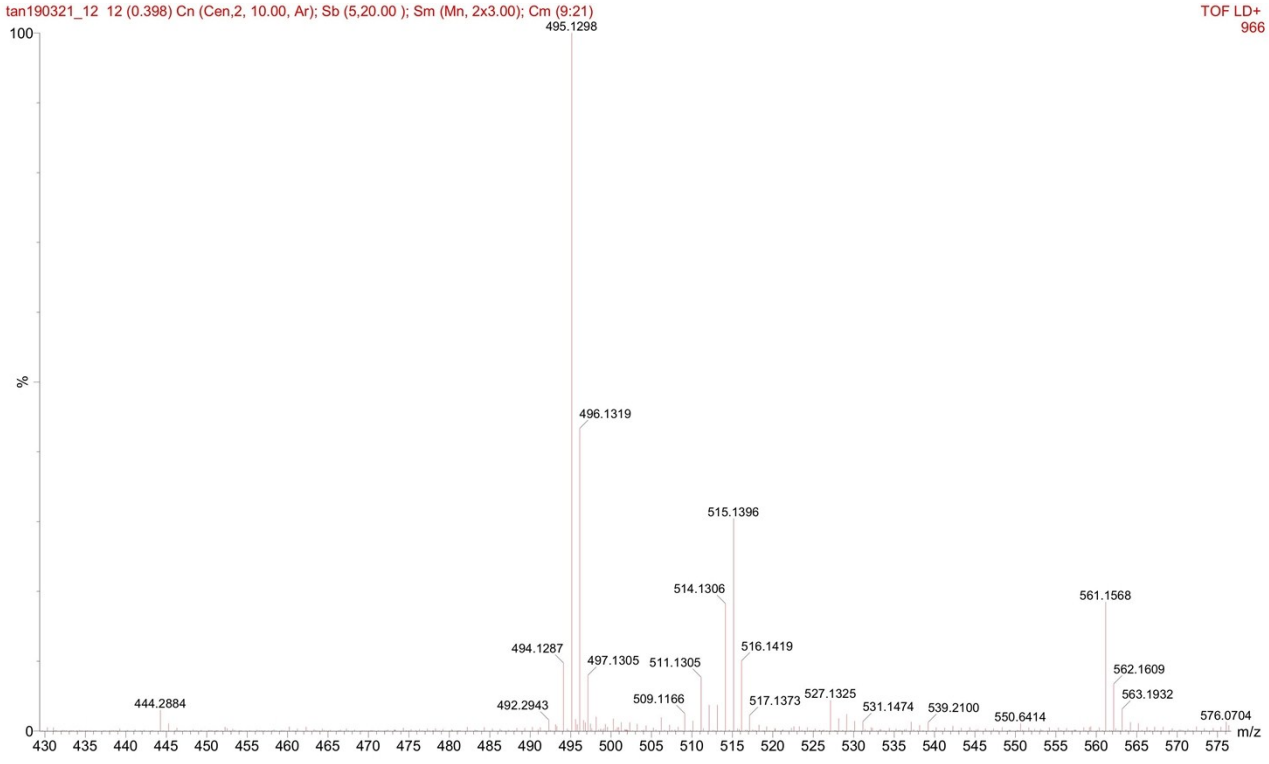

Figure S25. High-resolution mass spectrum of *c*-2FPCBO.

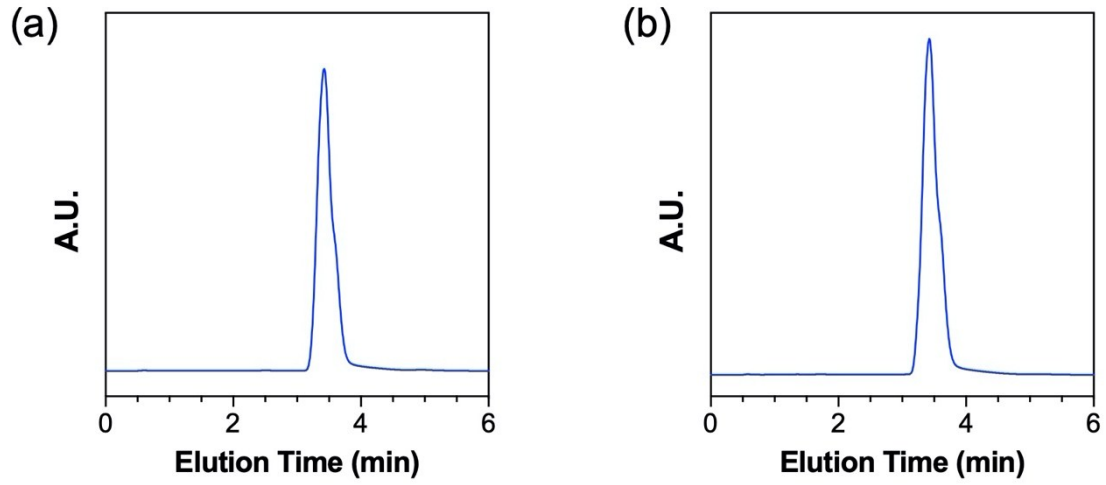

Figure S26. HPLC spectrum of (a) *t*-2FPCBO and (b) *c*-2FPCBO in acetonitrile solution.

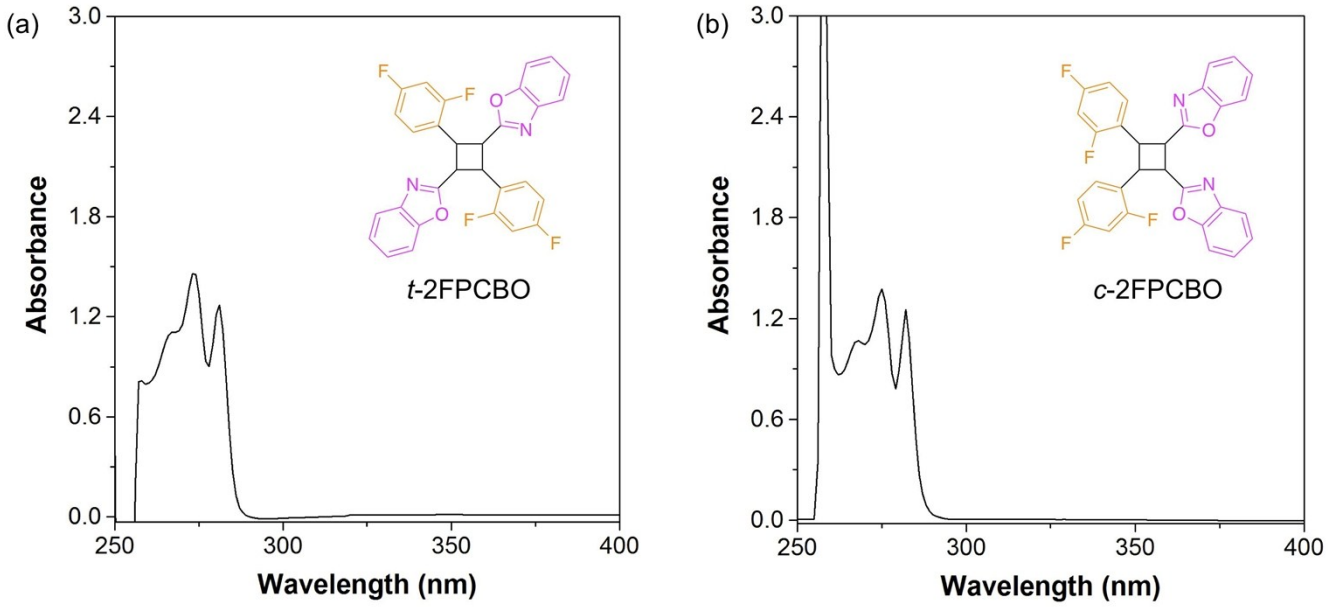

Figure S27. UV-vis absorption spectra of (a) *t*-2FPCBO and (b) *c*-2FPCBO in CH_2Cl_2. $c = 1.0 \times 10^{-5}$ M.

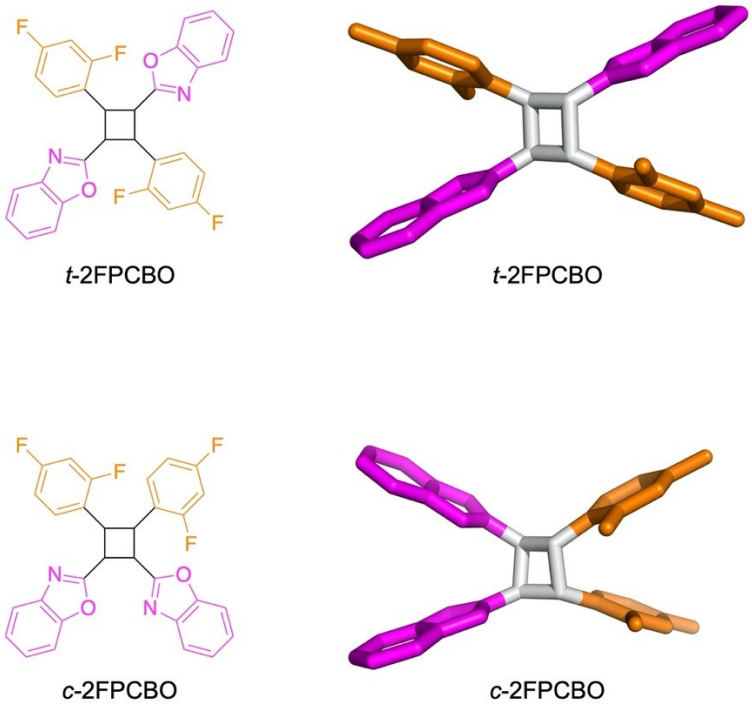

Figure S28. Crystal structures of *t*-2FPCBO and *c*-2FPCBO.

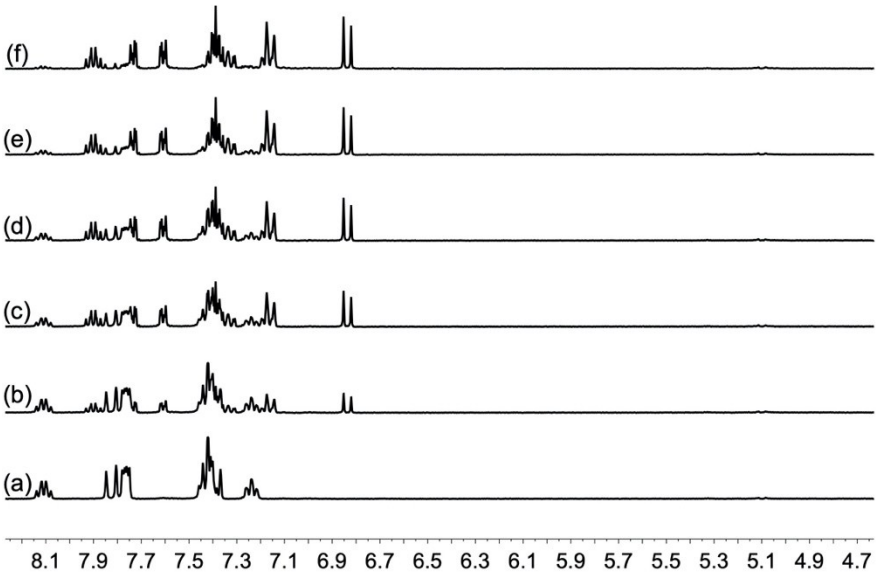

Figure S29. Partial ^{1}H NMR spectra (400 MHz, 298 K, DMSO-d_6) of *t*-2FSBO in DMSO-d_6 solution after irradiated by 365 nm UV for (a) 0 s, (b) 10 s, (c) 20 s, (d) 60 s, (e) 120 s, and (f) 300 s.

Table S2. Crystal data and structure refinement for *t*-2FPCBO, *c*-2FPCBO with blue emission and *c*-2FPCBO with yellow emission.

	t-2FPCBO	*c*-2FPCBO with blue emission	*c*-2FPCBO with yellow emission
CDCC	1942461	1942462	1942071
Formula weight	514.46	514.46	514.46
Sp. Group	P21/C	$P\bar{1}$	$P\bar{1}$
Crystal system	monoclinic	Triclinic	Triclinic
a (Å)	12.9258(2)	8.8798(6)	9.1590(3)
b (Å)	11.10764(16)	12.2737(10)	12.2660(5)
c (Å)	8.24353(13)	13.1272(12)	12.8671(6)
α (deg)	90	63.758(8)	107.066(4)
β (deg)	101.3647(16)	80.374(7)	107.962(4)
γ (deg)	90	68.947(7)	106.939(4)
V (Å^3)	1160.36(3)	1197.55(19)	1193.03(9)
Z	2	2	2
Dcalc (g/cm^3)	1.472	1.427	1.432
μ (mm^{-1})	0.975	0.944	0.948
Final R indices [I > 2sigma(I)]	R1 = 0.0333, wR2 = 0.0801	R1 = 0.0397, wR2 = 0.1013	R1 = 0.0452, wR2 = 0.1199
R indices (all data)	R1 = 0.0344, wR2 = 0.0808	R1 = 0.0505, wR2 = 0.1063	R1 = 0.0577, wR2 = 0.1276
GoF	1.053	1.094	1.055

Mechanism Behind the Phenomena

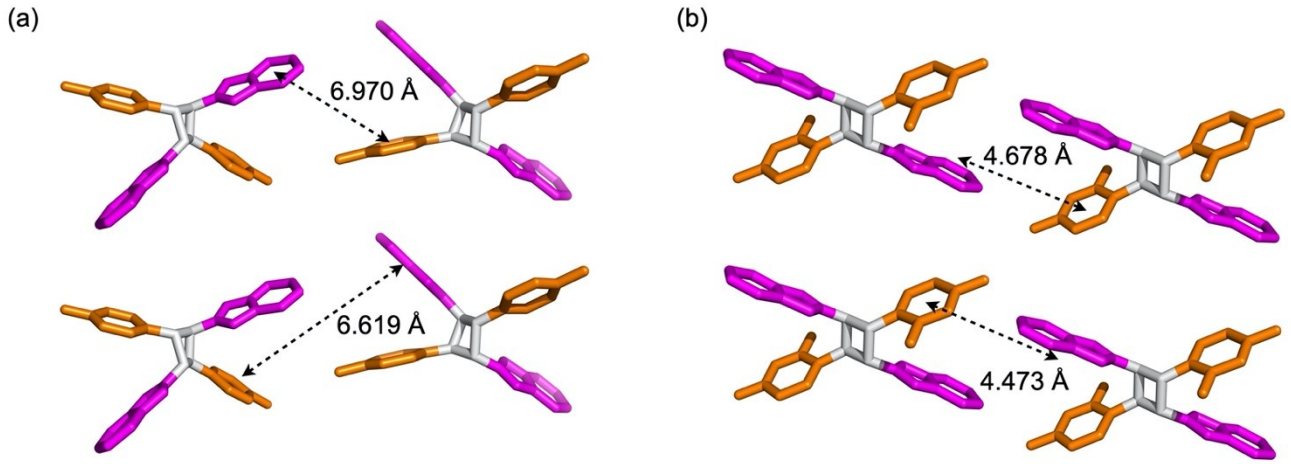

Figure S30. Crystal packing diagrams of (a) *t*-FPCBO and (b) *t*-2FPCBO.

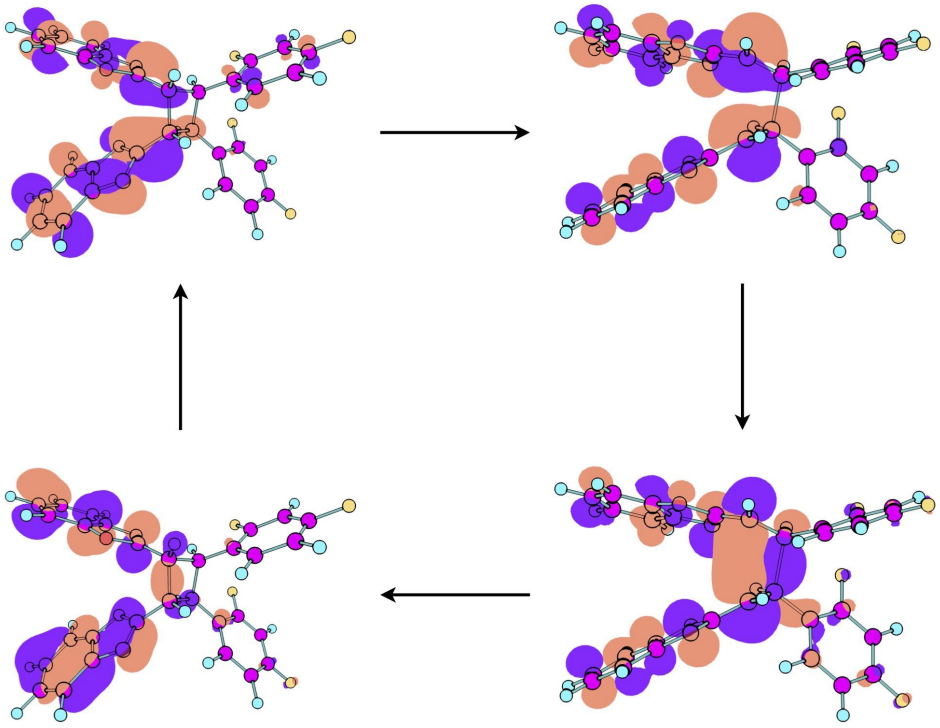

Figure S31. Electron cloud distribution, energy levels of *c*-2FPCBO in the excited state, ORCA 4.1 package.

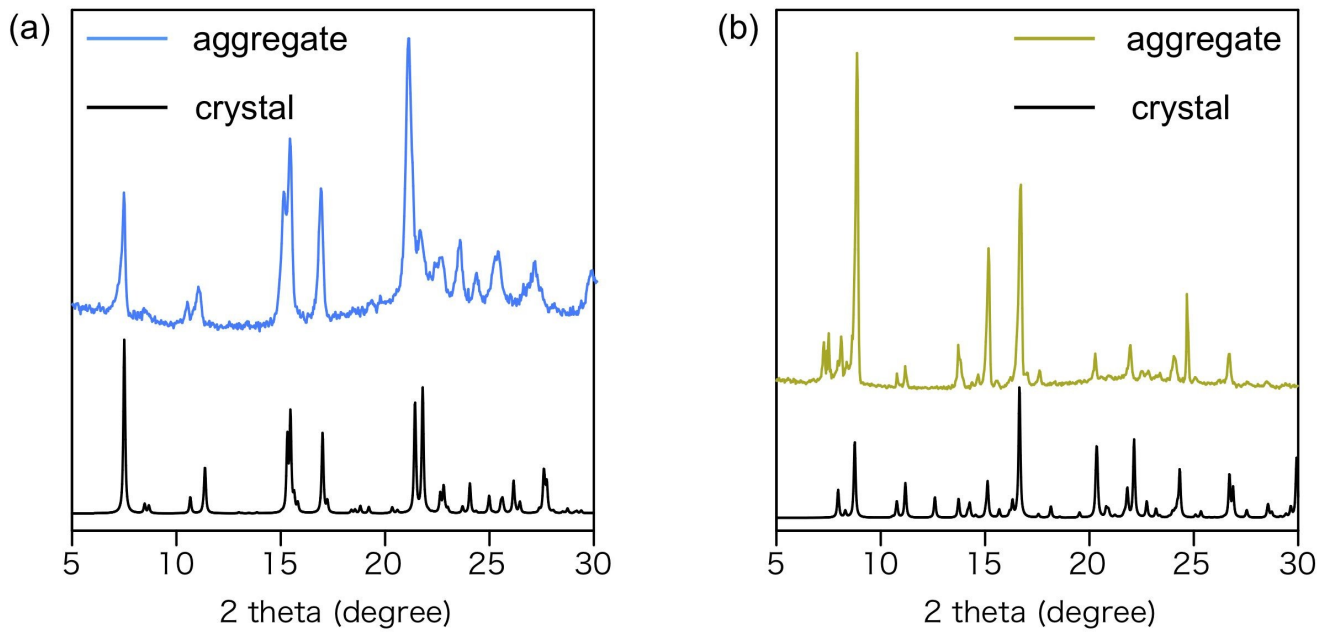

Figure S32. (a) XRD patterns of *c*-2FPCBO aggregates in DMSO/water mixture with 50% water fraction (blue line) and *c*-2FPCBO crystals with blue emission (black line). (b) XRD patterns of *c*-2FPCBO aggregates in DMSO/water mixture with 95% water fraction (yellow line) and *c*-2FPCBO crystals with yellow emission (black line).

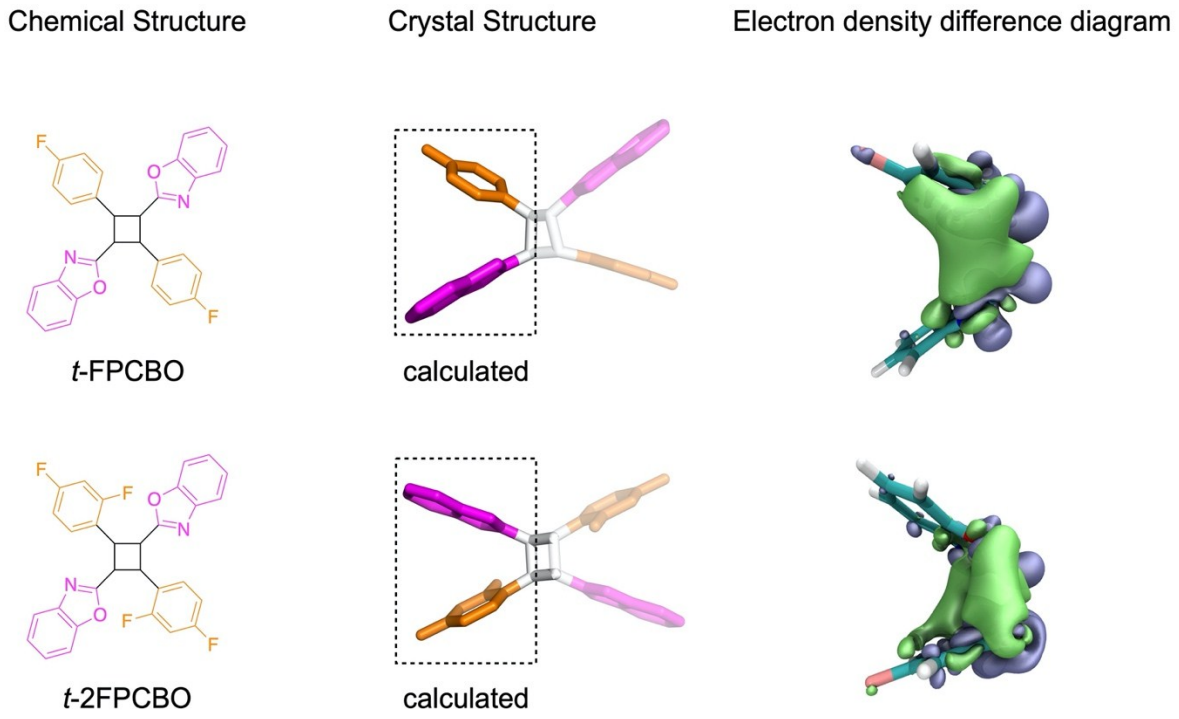

Figure S33. Electron density difference diagrams of partial structures of *t*-FPCBO and *t*-2FPCBO. Green part stands for increased electron density and purple part stands for decreased density.

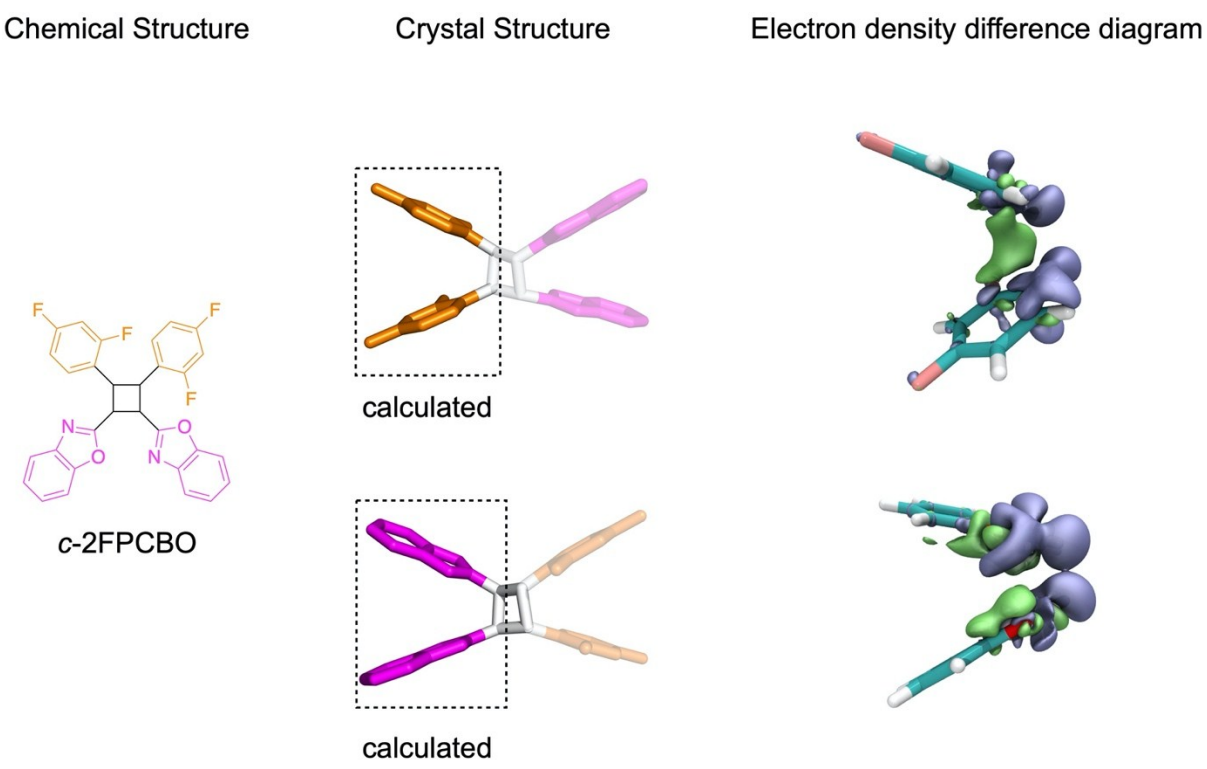

Figure S34. Electron density difference diagrams of partial structures of *c*-2FPCBO. Green part stands for increased electron density and purple part stands for decreased density.

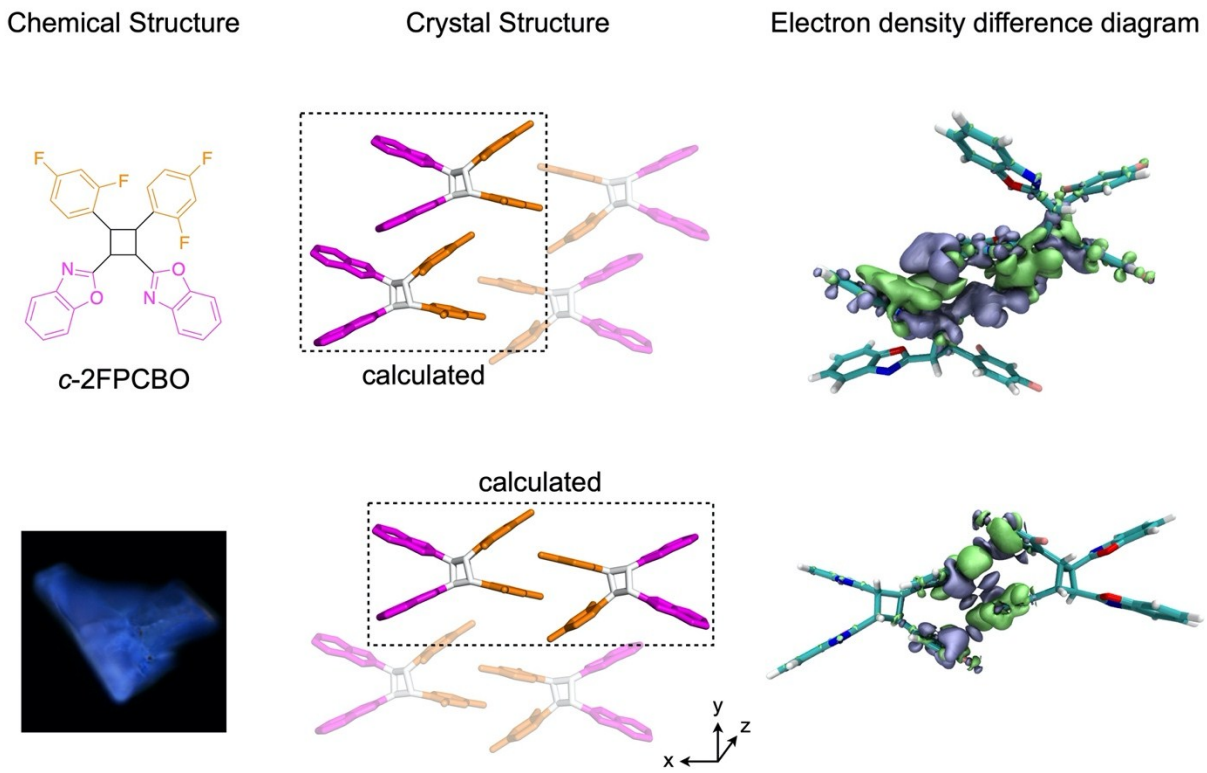

Figure S35. Electron density difference diagrams of partial structures of *c*-2FPCBO with blue emission. Green part stands for increased electron density and purple part stands for decreased

density.

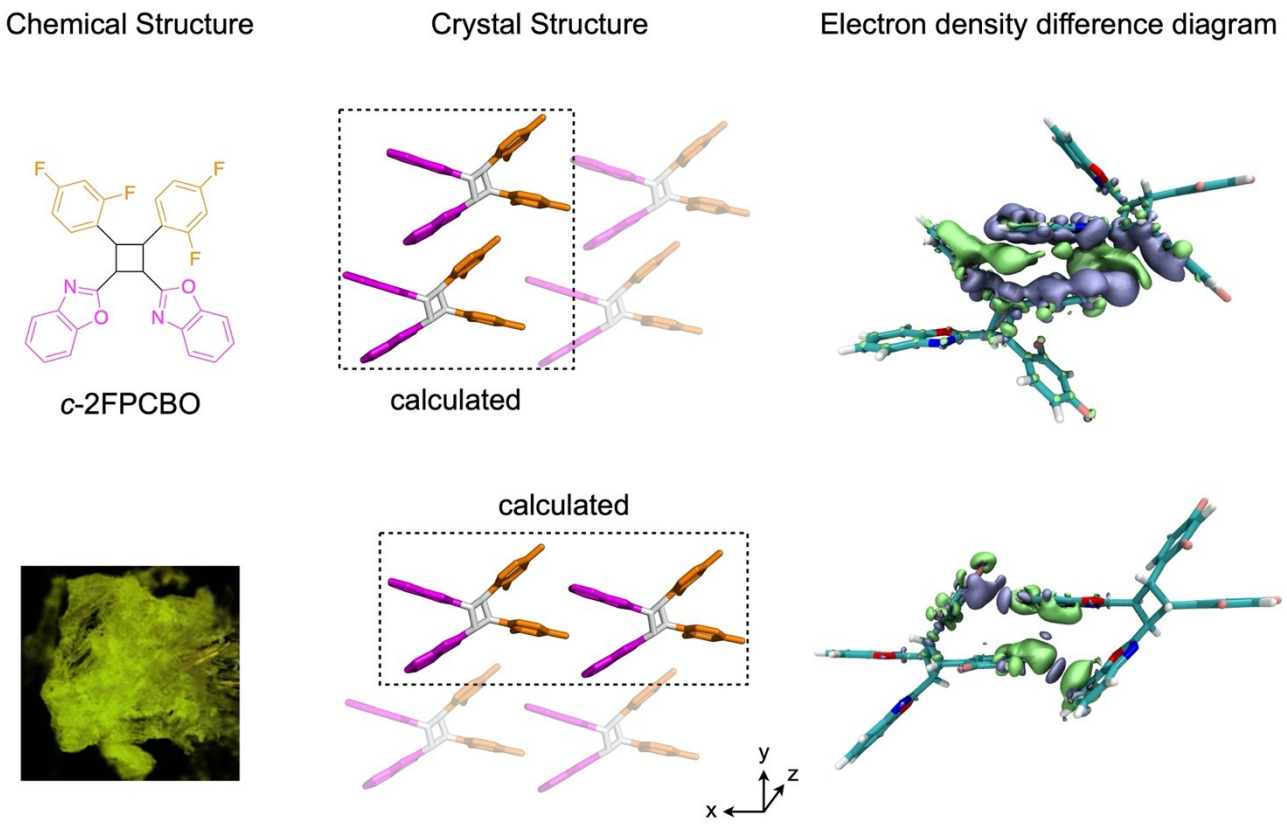

Figure S36. Electron density difference diagrams of partial structures of *c*-2FPCBO with yellow emission. Green part stands for increased electron density and purple part stands for decreased density.

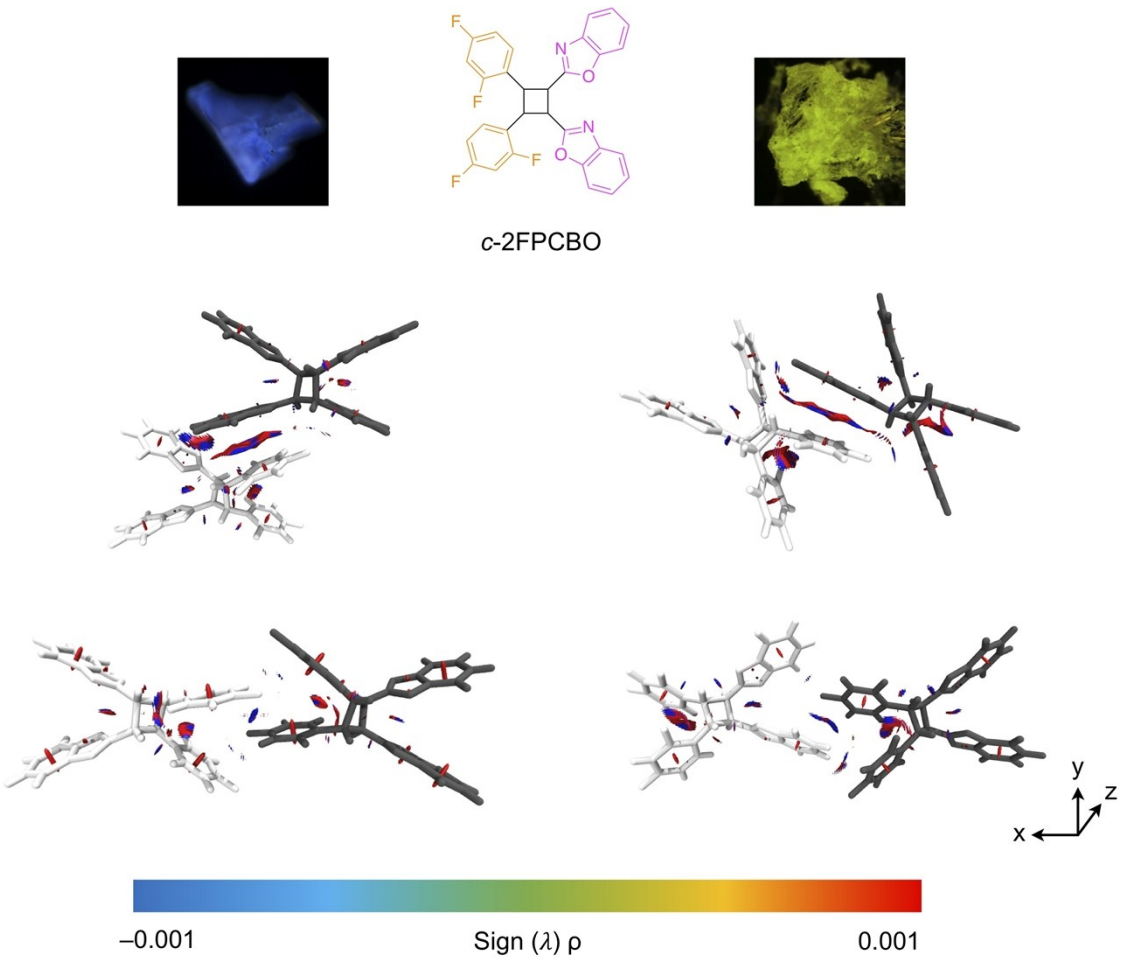

Figure S37. Two types of intermolecular non-bonding interactions in blue- and yellow-emissive *c*-2FPCBO crystals (RDG = 0.5).

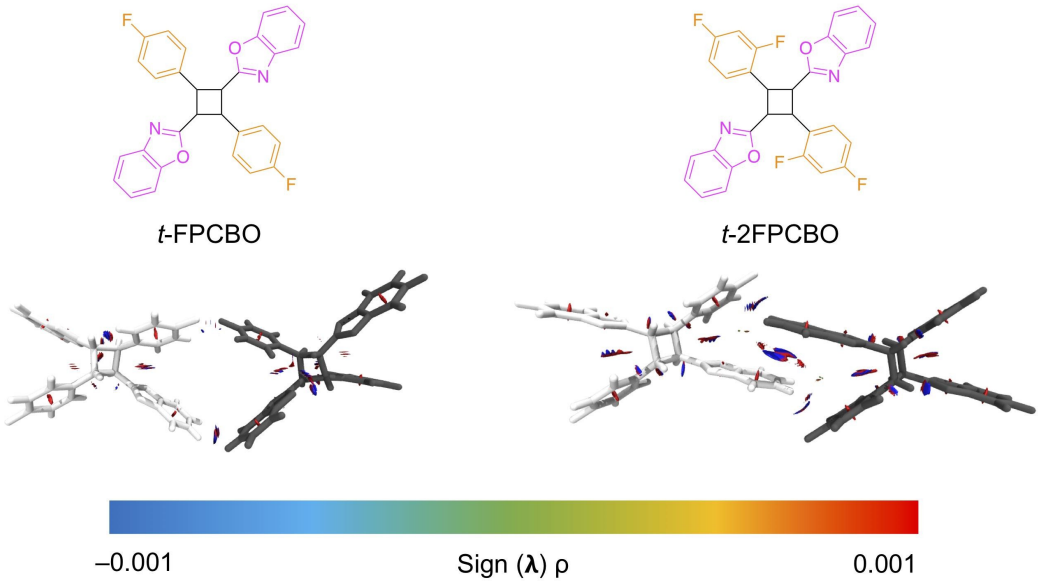

Figure S38. Intermolecular non-bonbing interactions in *t*-FPCBO and *t*-2FPCBO crystals (RDG = 0.5).

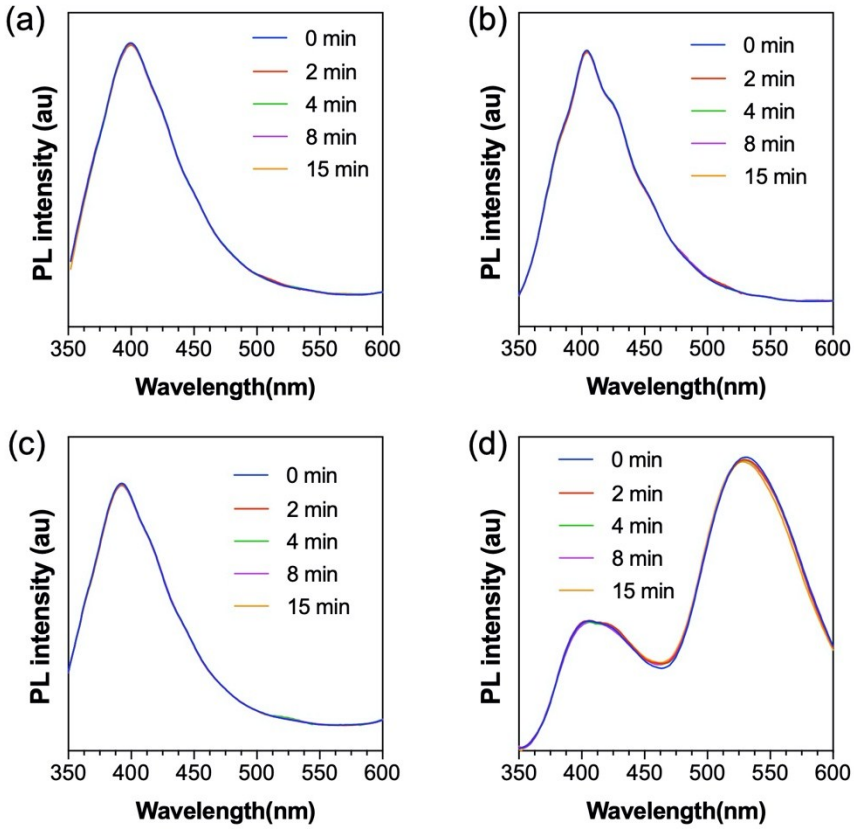

Figure S39. PL spectra of (a) *t*-FPCBO crystal, (b) *t*-2FPCBO crystal, (c) *c*-2FPCBO crystal with blue emission, and (d) *c*-2FPCBO crystal with yellow emission under UV irradiation for different time.

Table S3. Photophysical Properties of ***t*-FSBO**, ***t*-2FSBO**, ***t*-FPCBO**, ***t*-2FPCBO**, and ***c*-2FPCBO**

Compound	$\lambda_{abs,\ soln}$ (nm)[a]	$\lambda_{abs,\ solid}$ (nm)[b]	$\lambda_{em,\ soln}$ (nm)[c]	$\lambda_{em,\ aggr}$ (nm)[d]	$\lambda_{em,\ solid}$ (nm)[e]	$\Phi_{F,\ soln}$ (%)[f]	$\Phi_{F,\ solid}$ (nm)[g]
t-FSBO	324	325	392	396	426	0.4	0.2
t-2FSBO	325	320	394	400	459	2.5	1.0
t-FPCBO	273	274	403	411	395	0.1	2.8
t-2FPCBO	274	275	404	410	395	0.2	3.3
c-2FPCBO	274	275	405	416, 508	407, 528	0.2	3.2, 4.7

[a] $\lambda_{abs,\ soln}$ = absorption maximum in DMSO solution, $c = 1.0 \times 10^{-5}$ M. [b] $\lambda_{abs,\ solid}$ = absorption maximum in solid powder. [c] $\lambda_{em,\ soln}$ = emission maximum in DMSO solution, $c = 1.0 \times 10^{-5}$ M, λ_{ex} = 320 nm. [d] $\lambda_{em,\ aggr}$ = emission maximum in DMSO/water (*v*/*v* = 5/95) solution, $c = 1.0 \times 10^{-5}$ M, λ_{ex} = 320 nm. [e] $\lambda_{em,\ solid}$ = emission maximum in solid powder, λ_{ex} = 320 nm. [f] $\Phi_{F,\ soln}$ = fluorescence quantum yield in DMSO solution measured by an integrating sphere, $c = 1.0 \times 10^{-5}$ M, λ_{ex} = 320 nm. [g] $\Phi_{F,\ solid}$ = fluorescence quantum yield of solid powder measured by an integrating sphere, λ_{ex} = 320 nm.

Supplementary Videos

Supplementary Video 1. This video showed the "turn-on" behavior of a bulk *t*-FSBO crystal under 365 nm irradiation.

Supplementary Video 2. This video showed the "turn-on" behavior of *t*-FSBO crystal under 365 nm irradiation at vacuum and drycondition.

Supplementary Video 3. This video showed the *photosalient* behavior of *t*-FSBO microcrystals under 365 nm irradiation.

Supplementary Video 4. This video showed the *photosalient* behavior of *t*-2FSBO microcrystals under 365 nm irradiation.

Supplementary Video 5. This video showed the bending behavior of *t*-FSBO film on thinner glove irradiated by UV light. Upon withdrawing the UV light, the glove recovered to its original shape. Once the light source was provided, the glove could further re-bend.

Supplementary Video 6. This video showed the bending behavior of *t*-FSBO film on thicker glove irradiated by UV light. The bending degree was smaller when the substrate was thicker. Upon withdrawing the UV light, the glove recovered to its original shape. Once the light source was provided, the glove could further re-bend.

Supplementary Video 7. This video showed the disappearance of the bending behavior when there was no *t*-FSBO on glove.

References

[1] Wang, H.; Zhao, J.; Yang, G.; Zhang, F.; Sun, J.; Lu, R. *Org. Biomol. Chem.* **2018**, *16*, 2114.

[2] Sheldrick, G. M. SHELXL-97. Program Crystal Structure Refinement. University of Gottingen, Germany, 1997.

[3] Lu, T.; Chen, F. *Journal of Computational Chemistry* **2012**, *33*, 580.

[4] Lu, T.; Chen, F. *Journal of Molecular Graphics and Modelling* **2012**, *38*, 314.